Journal of Building Engineering 92 (2024) 109717

Contents lists available at ScienceDirect

Journal of Building Engineering

journal homepage: www.elsevier.com/locate/jobe

Computational design of isotropic and anisotropic ultralow thermal conductivity polymer foams

Janak Tiwari [a], Som S. Shrestha [b,**], Tianli Feng [a,*]

[a] Department of Mechanical Engineering, University of Utah, Salt Lake City, UT, 84112, USA
[b] Buildings and Transportation Science Division, Oak Ridge National Laboratory, Oak Ridge, TN, 37831, USA

ARTICLE INFO

Keywords:
Thermal insulation
Porous materials
Polymer foams
Finite element analysis
Effective medium approximation
Building energy efficiency
Foam blowing agents

ABSTRACT

Current state-of-the-art commercial polymer thermal insulation foam exhibits a thermal conductivity of 24 $mW{\cdot}m^{-1}{\cdot}K^{-1}$ (equivalently thermal resistivity of R-6/in.), similar to that of static air. To further optimize building energy efficiency, achieving even lower thermal conductivity is needed, which is, however, highly challenging. This paper presents computational evidence that demonstrates the feasibility of achieving an ultra-low thermal conductivity of less than 14.4 $mW{\cdot}m^{-1}{\cdot}K^{-1}$ (equivalently R-10/in.) using isotropic and anisotropic foam cell designs. For the isotropic design, we have identified analytical effective medium approximation (EMA) models within the accuracy of ±5% as finite element analysis (FEA) in predicting the effective thermal conductivity of foams with various porosities and filler gases. For the anisotropic design, we have developed and validated new EMA models against FEA in predicting the effective thermal conductivity of general anisotropic cuboids and Voronoi foams. For both isotropic and anisotropic designs, the design spaces for 18, 16, and 14.4 $mW{\cdot}m^{-1}{\cdot}K^{-1}$ (equivalently R-8, R-9 and R-10/in.) using various filler gases are obtained. It is found that polymer foams can be improved to achieve ultralow thermal conductivity by reducing CO_2 concentration, reducing radiation, increasing porosity, and using anisotropic pore geometry. These findings contribute to the development of highly efficient thermal insulation materials, enhancing building energy efficiency and promoting sustainable construction practices.

1. Introduction

Building energy consumption represents a substantial portion of total annual primary energy usage, accounting for approximately 40 % in the United States [1] and the European Union [2]. An enormous amount of energy is wasted through undesired heat transfer through building envelopes, which could be mitigated by developing high-performance thermal insulation materials. Not only for building envelopes [3–5], thermal insulation materials are also crucial for a wide range of applications, encompassing transportation pipelines for oil, water, and natural gas [6,7], aircraft, and reentry spacecraft [8,9], engine and exhaust systems in automobiles [10], refrigerators, freezers, tanks, and cold chain systems for vaccines [11–13]. Effective insulation of these engineering applications could save a significant amount of energy [14,15], decrease greenhouse gas emissions, enhance energy security, and lead to a sustainable future. Thus, the development of novel insulation methods with lower thermal conductivity is of great interest.

The heat transfer through the insulation material is quantified in terms of thermal conductivity or resistance to conduction (R-

* Corresponding author.
** Corresponding author.
E-mail addresses: shresthass@ornl.gov (S.S. Shrestha), tianli.feng@utah.edu (T. Feng).

https://doi.org/10.1016/j.jobe.2024.109717
Received 26 September 2023; Received in revised form 20 May 2024; Accepted 22 May 2024
Available online 23 May 2024

value/in.). It is common practice to use the R-value to quantify the insulation capability of foam in industry and construction settings, thus this paper employs thermal conductivity to quantify heat transfer and R/in. value to quantify the insulation capability of the foam. Fiberglass [16–18], vacuum insulation panels (VIP) [19–24], aerogels [9,25–27], mineral wools [28–30], and polymer foams [31–36] are commonly employed thermal insulation materials. Fiberglass is widely available, affordable, moldable, and fire-resistant, making it an excellent choice for commercial thermal insulation. However, it offers lower insulation capabilities with a thermal conductivity of approximately 40 $mW{\cdot}m^{-1}{\cdot}K^{-1}$ (equivalently R 3.6/in.). VIPs provide significantly higher insulation capabilities with ultra-low thermal conductivity of around 5.76 $mW{\cdot}m^{-1}{\cdot}K^{-1}$ (equivalently R-25/in. or more) but the lack of flexibility in fitting VIP insulation panels to specific building requirements, along with their fragility, high cost, and the need for effective sealing, limits their suitability for regular building envelope applications. Aerogels, characterized by their lightweight nature and nanostructured, highly porous composition, possess exceptional thermal insulation capabilities. They can be molded into various forms as needed for specific applications. Recent advancements in aerogel technology have introduced hydrophobic variants, which repel water moisture and maintain insulation performance over extended periods. Nevertheless, the fragility of aerogels renders them unsuitable for building envelopes that require mechanical integrity and strength. Mineral wools are easily available, cheap, and possess medium thermal and sound insulation capability, however, their heavy weight, health concerns, and moisture absorption limit their practical applications. Polymer foams, owing to their flexibility, affordability, lightweight nature, mechanical strength, moisture resistance, and sound absorption capabilities, remain the best choice and are widely used in building envelopes. However, commercially available polymer foams exhibit relatively lower insulation capabilities (approximately R-6/in.), prompting ongoing research efforts to enhance their thermal insulation performance.

The heat transport in porous materials is primarily governed by the conduction through solids and gases, as well as radiation. The effective thermal conductivity (k_{eff}) accounts for these contributions, with convection being negligible due to small pore sizes. It is important to note that solid and gas conduction, as well as radiation, are often coupled and studied together. There exists a trade-off between conduction through solids and gases and radiation heat transfer in porous materials [37,38]. Since solid has a higher thermal conductivity than gas, insulation foams usually require high porosity to reduce the solid thermal conductivity contribution. But it will simultaneously increase radiative thermal conductivity, leading to an overall increase in total thermal conductivity. Due to high porosity, the solid, gas, and radiation contributions are around 10, 70, and 20%, respectively, in polymer foams (e.g., high-density expanded polystyrene [38]). These numbers can change depending on specific foams. Reducing pore size can decrease the gas contribution, but it often results in a decrease in porosity (for a constant wall thickness), thereby increasing solid contribution. Lowering the pressure can reduce the gas contribution (such as in VIPs), but it requires the use of barrier films to prevent air leakage into the pores, which adds to the overall cost. Consequently, achieving a lower k_{eff} of thermal insulation materials while maintaining economic viability poses a challenge that necessitates a precise design.

This study aims to find possible ways to achieve ultra-low thermal conductivities for polymer foams with a target of 14.4 $mW{\cdot}m^{-1}{\cdot}K^{-1}$ using isotropic and anisotropic designs. The objective of this paper is three-fold. The first is to check the accuracy of existing effective medium approximation (EMA) models in predicting the effective thermal conductivity of isotropic foams, through a comparion with FEA simulations. The second is to develop a novel EMA model for anisotropic cuboid foams and Voronoi foams, since no EMA models are available for anisotropic foams. The third is to obtain the design space with ultra-low thermal conductivity of 14.4 $mW{\cdot}m^{-1}{\cdot}K^{-1}$ using isotropic and anisotropic foams and explore possible ways to reduce the effective thermal conductivity of polyiso foams. Polymer foams with ultralow thermal conductivity combined with their flexibility, lightweight, mechanical strength, moisture resistance, sound absorption capabilities, and affordability, would provide low-cost insulation solutions with better flexibility and mechanical strength and open a plethora of engineering applications.

The remainder of the paper is structured as follows. Section 2 provides a detailed explanation of the computational methodology. Section 3 focuses on isotropic foam designs. FEA simulations are conducted on various isotropic foams to identify accurate EMA models, which are used to delineate the design space for achieving R-10/in.-isotropic foams. Section 4 focuses on anisotropic foam designs. A new EMA model is developed and validated to accurately predict the effective thermal conductivity of anisotropic cuboid and Voronoi foams and obtain the design space for R-10/in.-anisotropic foams. Section 5 outlines some recommendations for enhancing the thermal conductivity of polyisocyanurate foams. Section 6 provides the conclusions.

2. Methodology

Several EMA models are available in the literature to predict the effective thermal conductivity of isotropic polyiso foams. Prior to utilizing EMA models, it is crucial to validate their accuracy against FEA. Consequently, we conduct FEA simulations on diverse foam structures, compare the results with various EMA models, and identify the EMA models that accurately predict thermal conductivity for isotropic foams. In the case of anisotropic foams, as no existing EMA models are available in the literature, we develop a novel EMA model based on anisotropic cuboid foams, which is subsequently validated through comprehensive FEA simulations. To enable the prediction of thermal conductivity for anisotropic Voronoi foams, more commonly encountered than cuboid foams, the new EMA model is improved based on the FEA simulations of various anisotropic Voronoi foams. As a result, accurate EMA models individually tailored for isotropic foams, anisotropic cuboid foams, and anisotropic Voronoi foams are obtained. These EMA models are applicable to diverse polymer matrix materials and gas fillers at varying concentrations.

For FEA simulations, the foams are generated by using Voro++, a 3D Voronoi structure generator [39,40]. The Voro++ coordinate output files are converted into Java scripts, which are inputted into COMSOL Multiphysics [41,42] to generate the geometry. For the isotropic structure, the pore size is uniform in all directions and takes the form of truncated octahedrons as shown in Fig. 1(a). The anisotropic structures are prepared by stretching the pore size along the Y and Z directions (perpendicular to the direction of heat

transfer) while keeping the pore size along the X direction (the direction of heat transfer) unchanged. The "anisotropic ratio" or "stretching ratio" is defined by the ratio between the pore size perpendicular to the heat transport direction and that along the heat transport direction. One should be careful that the wall thickness remains the same in all directions. The structures with an anisotropic ratio of 1.5 and 2 are shown in Fig. 1(b) and (c) respectively.

To calculate the effective thermal conductivity of foams at different porosities, parametric studies are conducted by adjusting the wall thickness of the aforementioned geometries using COMSOL Multiphysics' Heat Transfer Module. The simulation domain used in this study is displayed in Fig. 2. The left face and right face are maintained at fixed temperatures of 400 K and 300 K, respectively, along the X axis, which is also the heat flow direction as shown in the figure. The remaining faces were provided with periodic boundary conditions (assumed adiabatic). The model only accounts for conduction heat transfer through the solid walls and the gas, while neglecting the convection and radiation heat transfer. The solid walls were defined with the matrix property, while the gap between the solid walls (which acts as the pore) is defined with gas properties. To define boundary conditions, a cubical shell made of the same material as the solid walls of each geometry are encompassed around the array of each geometry. Tetrahedral meshing is used, with the governing Laplace's equation being solved at each node based on the specified boundary condition. The mesh density convergence study is carried out rigorously and is presented in the Supplemental information [43].

The thermal conductivity of the solid (matrix) material (k_m) is assumed to be 0.235 $W{\cdot}m^{-1}{\cdot}K^{-1}$ for the entire study. This value is taken as a representative case for the polyisocyanurate or polyurethane materials for which the bulk thermal conductivity lies between 0.160 and 0.260 $W{\cdot}m^{-1}{\cdot}K^{-1}$ [44–48]. The thermal conductivity of the filler gas (k_f) is varied. Here, we take the representative cases of 0, 0.011, 0.014, and 0.0265 $W{\cdot}m^{-1}{\cdot}K^{-1}$, which are labeled as vacuum, hydrofluoroolefin (HFO), pentane, and air, respectively. These thermal conductivity values cover the range of most common gases used in insulation foams. From the finite element simulations, the heat flux is calculated by using the surface integral of surface heat flux along the X direction on the right side. Similarly, the temperature gradient is obtained by performing the volume integral of the temperature gradient along the X direction of the entire domain. Using the surface heat flux and temperature gradient, effective thermal conductivity is calculated.

3. Designing ultra-low thermal conductivity isotropic foams

3.1. Validation of EMA models against FEA simulations on isotropic foams

In the industry, EMA models are commonly used to design polyiso foams due to their accessibility and user-friendliness. Unlike FEA, they do not require simulation expertise and offer computational efficiency, which is crucial for parametric study and industrial design optimization settings. These models also provide valuable insights into the physics of thermal transport in porous foam, allowing us to understand the impact of various parameters, such as matrix conductivity, gas conductivity, porosity, and pore geometry, on the effective thermal conductivity of the foam. As a result, multiple EMA models have been developed to predict the effective thermal conductivity of porous foam.

To find the EMA models that can accurately predict foam effective thermal conductivity, we have collected various existing EMA models in the literature, as shown in Table 1. These EMA models were developed for binary mixtures in different formats. For example, the Maxwell model describes the thermal conductivity of a mixture where a small volume fraction of isolated spherical particles is embedded inside the matrix material. The Russell model is developed for a matrix material embedded with orderly arranged cubes with any volume fraction. The Bruggeman model is improved from the Maxwell model for a high fraction of particle fillers. The Hashin and Shtrikman model is for the matrix embedded with percolated fillers. The Mori & Tanaka is for fiber-like or disk-like fillers. No matter how the matrix material is mixed with the filler material in what volume fraction, the mixture's effective thermal conductivity

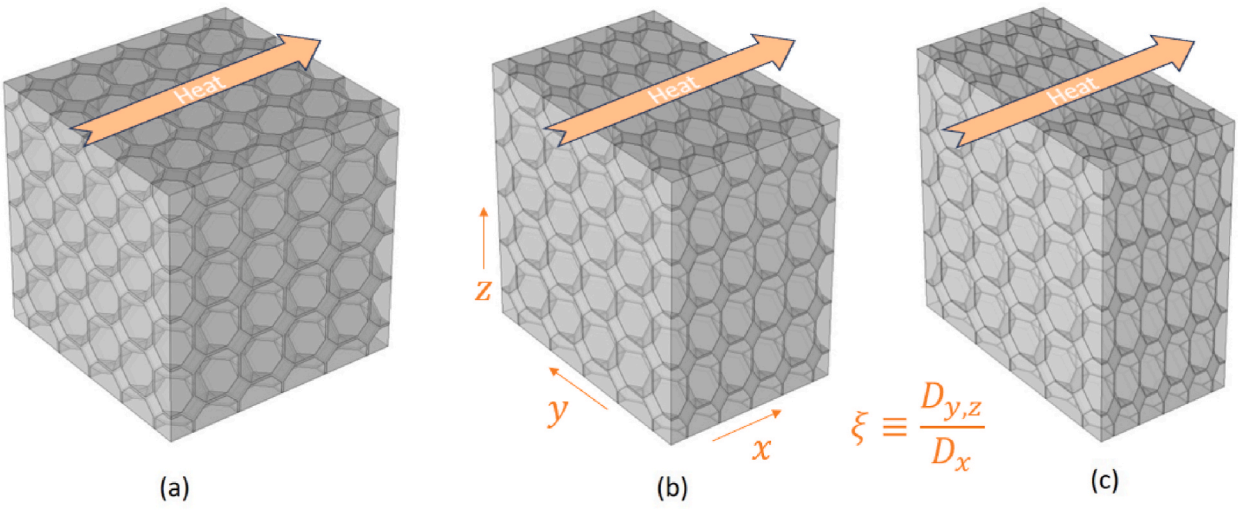

Fig. 1. Voronoi foams with different anisotropic ratios of 1 (a), 1.5 (b), and 2 (c). The anisotropic ratio is defined by the ratio between the pore size perpendicular to the heat transport direction and that along the heat transport direction. The cell wall thickness along x, y, and z directions are the same.

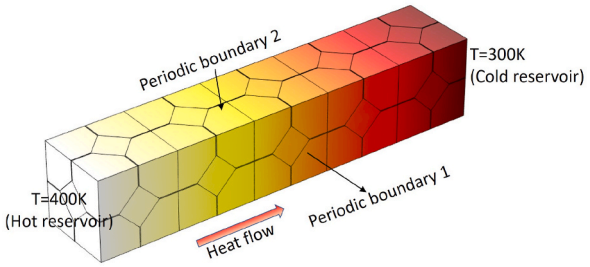

Fig. 2. Finite Element Analysis domain used in the study. Here, the anisotropic ratio is 1.

Table 1
Different effective medium approximation models to calculate the effective thermal conductivity of a binary mixture made of matrix material and fillers. k_f, k_m, and k_{eff} represent the thermal conductivities of the filler, matrix material, and binary mixture, respectively. φ is the volume fraction of filler.

Model	Equation	Comments
Upper limit [49]	$k_{eff} = \varphi k_f + (1-\varphi)k_m$	Parallel
Lower limit [49]	$k_{eff} = \left(\frac{\varphi}{k_f} + \frac{(1-\varphi)}{k_m}\right)^{-1}$	Series
Maxwell ($\varphi < 50$ %) [50,51]	$k_{eff} = k_m \frac{k_f + 2k_m + 2\varphi(k_f - k_m)}{k_f + 2k_m - \varphi(k_f - k_m)}$	For isolated particles
Russell [52]	$k_{eff} = k_m \left(\frac{(1-\varphi^{\frac{2}{3}}) + \frac{k_f}{k_m}\varphi^{\frac{2}{3}}}{1+\varphi-\varphi^{\frac{2}{3}} + \frac{k_f}{k_m}\left(\varphi^{\frac{2}{3}} - \varphi\right)} \right)$	embedded cubes (phase 2)
Decomposed Russell [38,52]	$k_{eff} = \varphi^{\frac{2}{3}} k_f + k_m \frac{1-\varphi^{\frac{2}{3}}}{1-\varphi^{\frac{2}{3}}+\varphi}$	
Bruggeman [53]	$\left(\frac{k_{eff}}{k_m}\right)^b \left(\frac{k_{eff}-k_f}{k_m-k_f}\right)\left(\frac{k_{eff}-k_0}{k_m-k_0}\right)^c = 1-\varphi,$	sphere particles, $\gamma = \frac{1}{3}$
	$b = \frac{3\gamma(\gamma-1)}{3\gamma+1}, k_0 = \frac{3\gamma+1}{3\gamma-5}k_f,$	prolate particles, $\gamma < \frac{1}{3}$
	$c = \frac{2(3\gamma-1)^2}{(3\gamma-5)(3\gamma+1)}$	oblate particles, $\gamma > \frac{1}{3}$
Hashin and Shtrikman [54]	$k_{eff} = k_f \left(1 - \frac{3(1-\varphi)(k_f-k_m)}{3k_f - \varphi(k_f-k_m)}\right)$	upper bound, Percolated fillers
	$k_{eff} = k_m \left(1 + \frac{3\varphi(k_f-k_m)}{3k_m + (1-\varphi)(k_f-k_m)}\right)$	lower bound, isolated fillers
Mori & Tanaka [55]	$k_{eff} = k_m + \frac{\varphi(k_f-k_m)\theta}{1-\varphi+\varphi\theta}$	fiber-like particles, $\theta = \frac{1}{3}\left(\frac{4k_m}{k_m+k_f}+1\right)$ spherical particles, $\theta = \frac{3k_m}{2k_m+k_f}$ disk particles, $\theta = \frac{1}{3}\left(\frac{k_m}{k_f}+2\right)$

must be located in between two limits. The upper limit is when the particle and matrix form parallel channels along the heat transfer direction, and the lower limit is when they align perpendicular to the heat transfer direction.

Thermal insulation foams can be viewed as a mixture of gas and solid, with gas being the filler material and solid being the matrix. The filler gas conductivity (k_f) may be inhibited by the pore size due to the Knudsen effect [56], i.e.,

$$k_f = \kappa_f^0 \left(1 + 2\beta\frac{\Lambda}{D}\right)^{-1}. \tag{1}$$

Here k_f^0 is the diffusive limit of gas thermal conductivity at a given temperature T. β is a parameter determined by the energy exchange rate between solid and gas molecules, $\beta = \beta_0 \cdot \frac{2-\alpha}{\alpha}, (0 \le \alpha \le 1)$, where α is the energy accommodation coefficient between the gas molecules and the solid material [57]. Λ is the gas molecules' mean free path given by $\Lambda = \frac{k_B T}{\sqrt{2}\pi d^2 P}$. P is pressure, T is temperature, D is pore size, d is the kinetic diameter of the gas molecules, and k_B is the Boltzmann constant. In the case when the gas is made of multiple gas species, the gas thermal conductivity should be calculated as:

$$k_f = \sum_{i=1}^{n} \frac{x_i}{\sum_{j=1}^{n} x_j A_{ij}} k_{f_i}. \tag{2}$$

Here x_i and k_{f_i} are the molar fraction and thermal conductivity of the gas species i. n is the total number of gas species. A_{ij} is the interaction parameter between gas species i and j, which can be calculated with the Mason-Saxena equation as explained in Ref. [58]. When there is a Knudsen effect, k_{f_i} should be calculated by using Eq (1), where the pressure P should still be the total pressure of the gas rather than the partial pressure of the species i. Throughout this paper, the Knudsen effect of gas thermal conductivity is not considered in the FEA simulations since the smallest pore size that can be achieved in practical commercial applications is hundreds of microns, which are much larger than the gas molecules' mean free path at ambient pressure.

To identify the EMA models that can accurately predict the effective thermal conductivity of foams, we conduct FEA simulations and obtain the thermal conductivity of polyisocyanurate foams at various filler volume fractions (porosities), as shown in Fig. 3. These results are compared with all the EMA models. Here, we consider two fillers, i.e., vacuum ($k_f = 0$) and HFO ($k_f = 0.011$ W·m^{-1}·K^{-1}). Additionally, the finite element study of Amit et al. [59] on vacuum porous insulation foam is included for reference. Our result aligns well with their results. It is evident that, except for the upper model, lower model, Bruggeman model, and Mori and Tanaka (fiber) model, all other EMA models align well with the FEA results. Therefore, it is safe to pick any of the Russell, decomposed Russell, Maxwell, Mori and Tanaka (sphere), and HS models to predict the thermal conductivity of foams. Throughout the remaining sections of this paper, we use the decomposed Russell model, similar to our recent work [38]. The results are continuously compared to FEA to ensure accuracy.

3.2. R-value of isotropic polymer foam with various blowing agents

With the decomposed Russell model, we obtain the thermal conductivity and R-value of polymer foams filled with various gases as shown in Fig. 4. The figure demonstrates that the decomposed Russell accurately calculates the effective thermal conductivity. The different gases have thermal conductivities ranging from 0 (for vacuum) to 0.026 W·m^{-1}·K^{-1} (for air). Note that these analyses assume radiation is eliminated and thus represent the upper limit of R-value (or lower limit of thermal conductivity) that can be achieved in polymer foams, assuming pore size is not small enough to create the Knudsen effect.

Considering the common range of polymer insulation foam porosity, 95–98%, the highest R-values by using air, pentane, and HFO are R-5/in., R-8.5/in., and R-10.3/in., respectively. This indicates that R-10/in. is feasible under the commercial production capabilities: large pore size, porosity of 97.6%, and ambient pressure, if the radiation can be eliminated, for example, by opacifiers.

3.3. Design space for isotropic foams with R-8/in., R-9/in., and R-10/in

Using the decomposed Russell model, we have predicted the design spaces of isotropic foams with R-values of R-8/in., R-9/in., and R-10/in., as shown in Fig. 5. Figures (a, c, and e) assume zero radiation, while Figures (b, d, and f) assume 20% radiation to the effective thermal conductivity, which is a commonly reported value [60–63] for polyisocyanurate foams. This comparison allows us to visualize the impact of radiation on thermal transport. The design spaces are shown in the shaded areas. For instance, any polyisocyanurate foam lying inside the green area has an R-value not less than R-10/in.

Fig. 5(a) and (b) illustrate the design spaces for isotropic open-cell polyisocyanurate foams (filled with air) with 0 and 20% radiation contributions, respectively. It is evident that achieving R-8/in., even when neglecting radiation contribution, requires restricting the pore size to the sub-micron scale. As shown in Fig. 5(c), when transitioning from an open-cell design to a closed-cell design with pentane (k_f of 0.014 W m^{-1}·K^{-1}) as filler gas, an R-8/in. can be attained with a pore size of approximately 50 μm, given a porosity of around 98% and no radiation contribution. However, to achieve R-10/in., the pore size needs to be further reduced to the submicron level. As shown in Fig. 5(d), considering a radiation contribution of 20 %, achieving even an R-8/in. value necessitates decreasing the pore size to submicron dimensions when using pentane as the blowing agent. Fig. 5 (e) and 5(f) present the design spaces using HFO as the filler gas. Remarkably, even with bulk-sized pores (pore size >100 μm), we can attain R-10/in. when

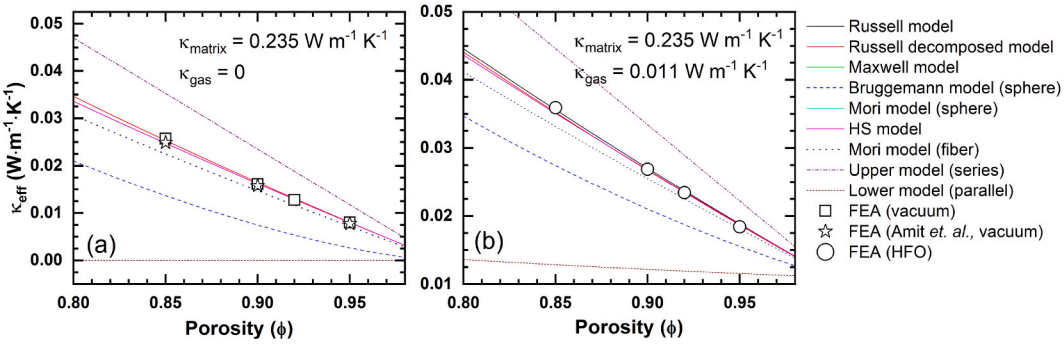

Fig. 3. Comparison of effective thermal conductivity obtained from different EMA models with the finite element analysis results. The matrix material is taken as polyisocyanurate ($k_m = 0.235$ W·m^{-1}·K^{-1}), and the filler gas is taken as (a) vacuum ($k_f = 0$ W·m^{-1}·K^{-1}) and (b) HFO ($k_f = 0.011$ W·m^{-1}·K^{-1}).

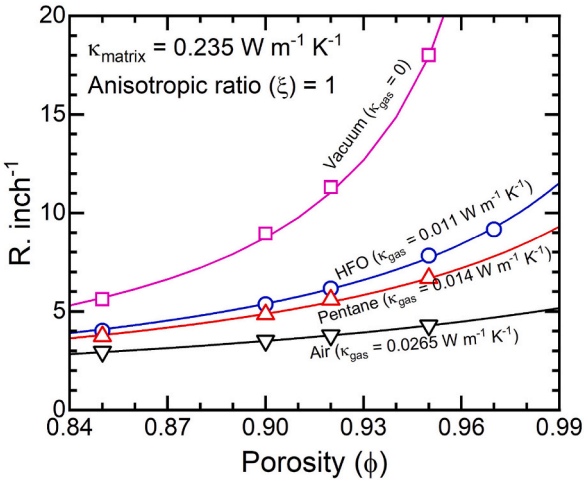

Fig. 4. Comparison of finite element analysis results with the decomposed Russell model for different gases and porosities. Radiation contribution to thermal conductivity is assumed to be eliminated. The Knudsen effect is not considered, assuming the pore size is much larger than the molecule mean free path.

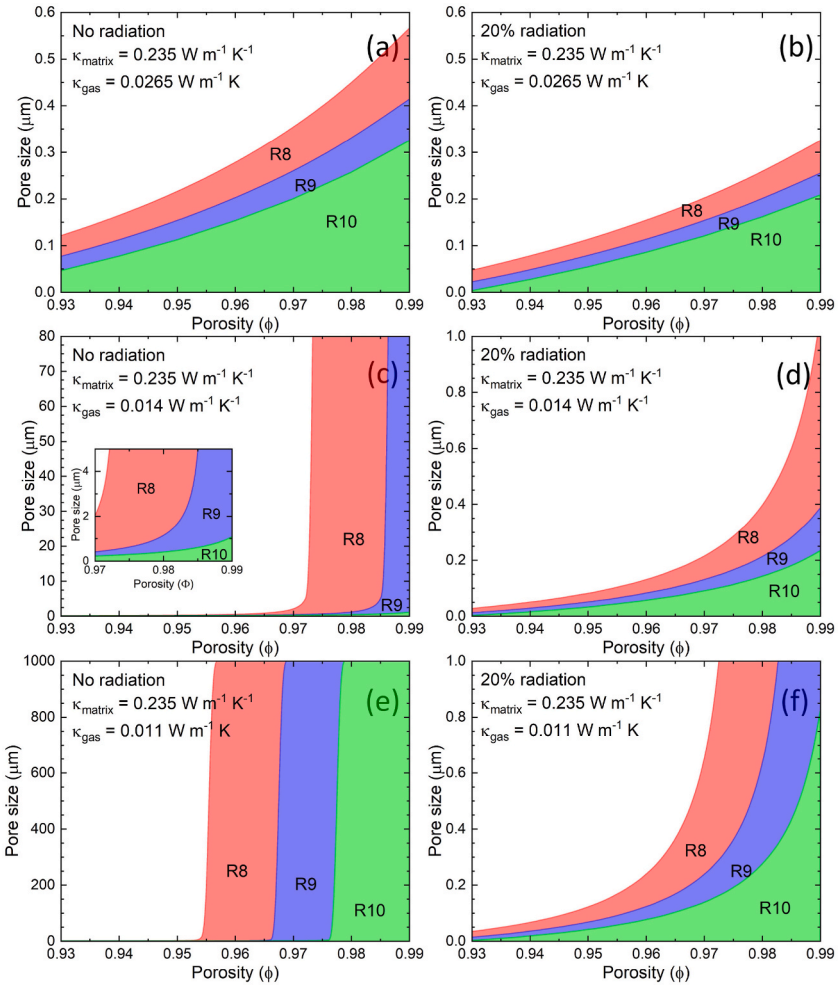

Fig. 5. R-10/in. design space for isotropic polyisocyanurate foams filled with (a) air with no radiation, (b) air with 20% radiation, (c) pentane with no radiation, (d) pentane with 20% radiation, (e) HFO with no radiation, (f) HFO with 20% radiation. Here, air, pentane, and HFO are taken as representative gases with thermal conductivity of 0.0265, 0.014, and 0.011 $W{\cdot}m^{-1}{\cdot}K^{-1}$, respectively.

radiation is diminished. However, achieving this high R-value necessitates a porosity as high as 97.6%. Achieving R-8/in. becomes relatively easier with a porosity of 95%. Nevertheless, when the radiation contribution is considered, a shift towards submicron pore sizes becomes imperative. This is due to the balance between the increase in k_{eff} caused by radiation contribution and the decrease in k_{eff} resulting from a reduction in gas contribution due to the Knudsen effect. Hence, the figure underscores the crucial role of diminished radiation in realizing an R-10/in. value.

4. Designing ultra-low thermal conductivity anisotropic foams

4.1. Development of EMA model for anisotropic cuboid foams

As no existing EMA models for anisotropic foams are available in the literature, we develop an EMA model based on anisotropic cuboid foams, as shown in Fig. 6 (b). The derivation method is similar to that of Russell model, and the details are shown in the Supplemental information [43]. The effective thermal conductivity (k_{eff}) of anisotropic cuboid foams as a function of the anisotropic ratio "ξ", porosity "φ", gas thermal conductivity "k_f", and solid thermal conductivity "k_m" is derived as

$$k_{eff}(\varphi,\xi,k_m,k_f) = (1+x)\left[xk_m^{-1} + \left(k_m - \varphi(1+x)(k_m-k_f)\right)^{-1}\right]^{-1}. \tag{3}$$

Here, the factor x is obtained by solving $(1+x)(\xi+x)^2 = \frac{\xi^2}{\varphi}$ and can be totally determined by ξ and φ as

$$x = \frac{1}{3}\left(a + \frac{(\xi-1)^2}{a} - 2\xi - 1\right), \tag{4}$$

$$a = \left(\frac{3}{2}\left(12\frac{(\xi-1)^3\,\xi^2}{\varphi} + 81\frac{\xi^4}{\varphi^2}\right)^{\frac{1}{2}} + (\xi-1)^3 + \frac{27}{2}\frac{\xi^2}{\varphi}\right)^{\frac{1}{3}}. \tag{5}$$

The new EMA model for anisotropic foam is easy to use. The only extra parameter introduced in Eqs. (3)–(5) as compared to the existing EMA models in Table 1 is the anisotropic ratio ξ ($\xi \geq 1$).

4.2. Finite element simulations of anisotropic cuboid foams

To validate the new EMA model, Eqs. (3)–(5), for anisotropic cuboid foams, we perform the FEA simulations. As seen in Fig. 7, a good agreement between our new EMA model and FEA results is found, demonstrating the reliability of the new EMA model. From the result, we find that anisotropic design can effectively reduce thermal conductivity. For example, when the gas is HFO, an anisotropic ratio of 2 can increase the R-value from R-5.44/in. to R-6.21/in. at 90% porosity. For air, the increase is from R-3.45/in. to R-3.73/in. In a porous structure, a substantial portion of heat transfer occurs through the matrix structure, which acts as a network of bridges for heat transfer. The anisotropic foam design decreases the number of connecting bridges along the direction of heat transfer and thus helps reduce thermal conductivity and increase the R-value.

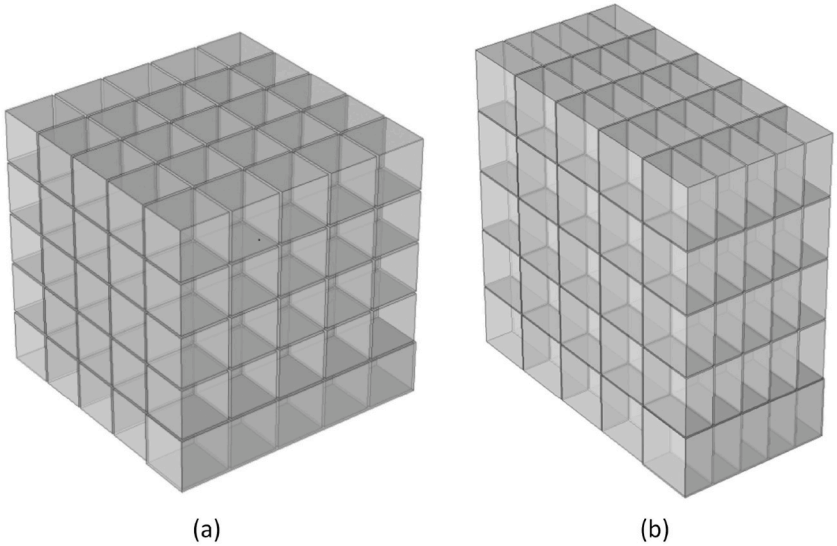

Fig. 6. Cuboid polyisocyanurate foam design. (a) isotropic (anisotropic ratio = 1) and (b) anisotropic ratio = 2. Heat transfer is from left to right.

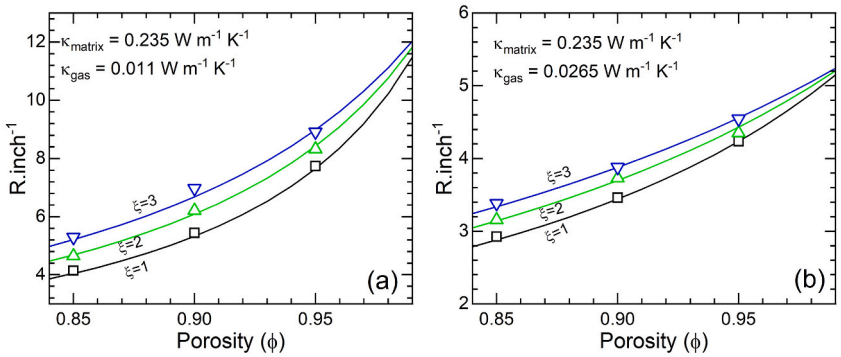

Fig. 7. R values obtained from our developed EMA model (Eqs. (3)–(5)) and FEA simulations for anisotropic cuboid foams filled with (a) HFO and (b) air. Results of anisotropic ratios of 1,1.5 and 2 are shown.

4.3. *Improvement of the EMA model for anisotropic Voronoi foams*

While our new EMA model accurately predicts the effective thermal conductivity of anisotropic cuboid foam, it does not accurately predict that of anisotropic Voronoi foams. This is because our new EMA model assumes perpendicular heat flow paths as in the cuboid foam, which is not the case in Voronoi foams. Further modifications to the EMA model are necessary to accommodate the intricate geometry and heat transfer mechanisms specific to Voronoi structures. Therefore, we perform FEA analysis and obtain the thermal conductivity of various anisotropic Voronoi structures as shown in Fig. 8. After the fitting, we figure out that the effective anisotropic ratio of Voronoi structures should be that of cuboid structure to the power of 1.8. This power of 1.8 on the anisotropic ratio accounts for the more distorted heat flow path in the anisotropic Voronoi structure compared to the anisotropic cuboid structure. Thus, after replacing ξ with $\xi^{1.8}$ in Eqs. (3)–(5), the model can well predict the thermal conductivity of anisotropic Voronoi foams, as shown in Fig. 8.

Therefore, the EMA model that works for anisotropic Voronoi foams is given by Eq. (3), with x and a calculated by ξ and φ as

$$x = \frac{1}{3}\left(a + \frac{\left(\xi^{1.8}-1\right)^2}{a} - 2\xi^{1.8} - 1\right), \tag{6}$$

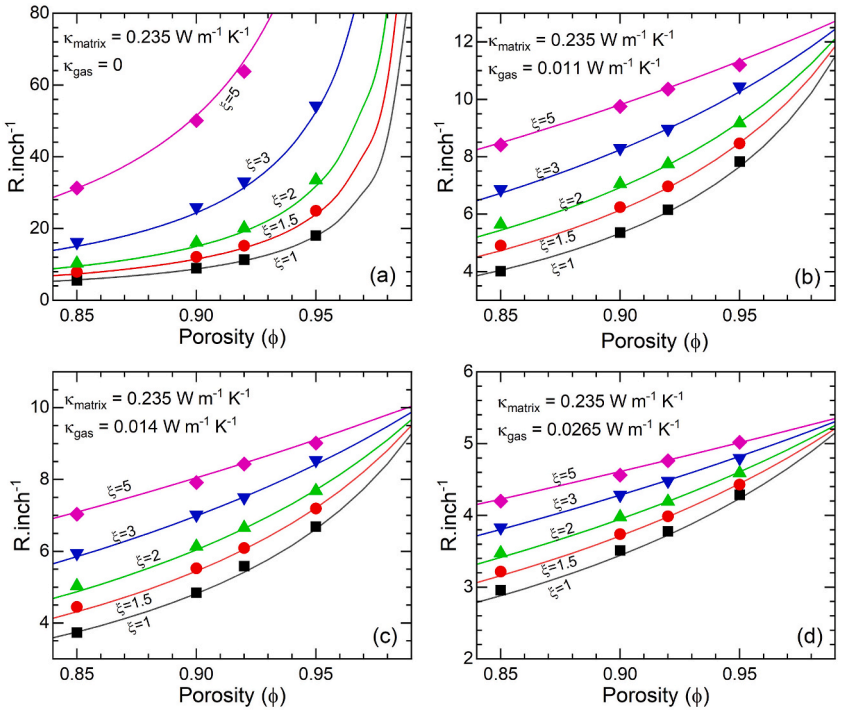

Fig. 8. Effective thermal conductivity of the anisotropic Voronoi polyisocyanurate foam obtained using finite element analysis and our developed EMA model (Eqs. (3), (6) and (7)). The matrix material is taken as polyisocyanurate, and the filler gas is taken as (a) vacuum, (b) HFO, (c) pentane, and (d) Air.

$$a = \left(\frac{3}{2}\left(12\frac{\left(\xi^{1.8}-1\right)^{3}\xi^{3.6}}{\varphi}+81\frac{\xi^{7.2}}{\varphi^{2}}\right)^{\frac{1}{2}}+\left(\xi^{1.8}-1\right)^{3}+\frac{27}{2}\frac{\xi^{3.6}}{\varphi}\right)^{\frac{1}{3}}. \quad (7)$$

It is understandable that the effective anisotropic ratio of anisotropic Voronoi foam is larger than that of anisotropic cuboid foams. The anisotropic ratio in determining thermal conductivity is a representation of how heat transfer is blocked by walls. When the foam is made of parallel alternative polymer and gas walls, the anisotropic ratio is infinite. In this case, the thermal conductivity is lowest. That is, the higher the anisotropic ratio, the lower the thermal conductivity, and the more distorted the heat transfer path is. Therefore, Voronoi foams have a more substantial anisotropic effect than cuboid foams since the heat transfer path in Voronoi foams is more distorted or blocked. Fig. 8 shows that anisotropic design is more beneficial at lower porosity and for higher matrix-filler material thermal conductivity ratio. For example, an anisotropic ratio of 2 can increase the R-value of air-filling foams by 86% and HFO-filling foams by 17.3%.

4.4. R-10 merit diagram of Voronoi anisotropic foams

Fig. 9 shows the R-10/in. design space for anisotropic Voronoi foams at different radiation contributions. Anisotropic design reduces the effective thermal conductivity and makes it much easier to achieve R-10/in. For isotropic design, porosity needs to be as high as 97.6% to achieve R-10/in., when considering diminished radiation and 600 μm pore size. The porosity needed is decreased to 97.2% and 96.2% when using the anisotropic ratio of 1.5 and 2, respectively. Even with a 10% radiation contribution, it is possible to achieve R-10/in. at bulk pore size when the anisotropic ratio is 2. However, when the radiation contribution increases to 20%, pore size needs to be less than 2 μm to achieve R-10/in., even with an anisotropic ratio of 2.

5. Guidance to experiment

Our results can provide guidance to experimental designs. We have made polyisocyanurate foam samples and achieved the highest R-value of R-7/in. with a porosity of 96%, as the red star shown in Fig. 10. The sample has an isotropic Voronoi structure filled with HFO and CO_2. Based on our simulation results, we propose that the R-value of the sample can be further improved in the following ways.

First, the R-value can be improved by diminishing radiation contribution to thermal conductivity. The blue dashed curve and blue diamond show the R-value of the experimental sample at diminished radiation, calculated using the decomposed Russell model and FEA simulations, respectively. It is found the R-value can be improved from R-7/in. to 7.74/in. when the radiation is eliminated, which can be done by adding different opacifiers [64–66] such as silica, carbon black, carbon nanotubes, etc., during the foaming process. Second, the R-value can be improved by increasing porosity. As shown by the blue dashed curve, the R-value can be further increased from 7.74 to 8.85 when porosity increases from 96% to 97.5%, which is a common porosity in commercial polyisocyanurate foams. This is because of the decrease in solid contribution with an increase in porosity. Porosity can be controlled by altering the foaming process and concentration of different constituents. Third, the R-value can be improved by eliminating CO_2 in the filler gas or by using filler gases with lower thermal conductivity. The magenta dashed curve shows the R-value of the same foam but without CO_2 (still without radiation), calculated using the decomposed Russell model. The results agree well with the FEA simulations, shown as magenta crossed circles. The R-value increases from 8.85 to 9.76 at 97.5%. The concentration of CO_2 in the filler gas can be decreased by controlling its generation during the foaming process, which can be done by controlling the amount of water during foaming. Last but not least, the R-value can be improved by increasing the anisotropic ratio. As shown by the red dashed line with red rectangular symbols, the R-value can be improved from 9.76 to 10.86 at 97.5% porosity if the anisotropic ratio is increased from 1 to 2. This can be done experimentally in several ways, as seen in the literature [67–70]. In summary, the R-value of the porous foam can be increased by: (a) diminishing the radiation, (b) increasing the porosity, (c) eliminating the CO_2 in the filler gas, and (d) using anisotropic pores.

6. Conclusions

This study explores the feasibility of designing polymer foams with an ultra-high R-value (i.e., R-10/in.) by using FEA simulations and EMA models. We start with the traditional isotropic foam design and then dive into the more advantageous anisotropic design. For isotropic foams, the accuracy of various existing EMA models is examined through a comparison with FEA simulations. It is found that the Russell, decomposed Russell, Maxwell, Mori and Tanaka (sphere), and HS models are accurate within the error margin of ±5%. Using the validated EMA models, we have obtained the design space of R-8/in., R-9/in., and R-10/in. isotropic foams filled with vacuum, HFO, pentane, and air, separately. Considering the practically achievable porosity (95–98%), the highest R-values by using air, pentane, and HFO are R-5/in., R-8.5/in., and R-10.3/in., respectively. For example, to achieve R-10/in., the porosity needed for HFO-filled foam is 97.6%, which is practically feasible. For the anisotropic foam design, new EMA models are developed and validated, which can accurately predict the effective thermal conductivity of anisotropic cuboids and Voronoi foams. Anisotropic design helps to increase the R-value and makes it easier to achieve R-10/in. Increasing the anisotropic ratio from 1 to 2, the R-values of foams filled with vacuum, HFO, pentane, and air increase from R-18/in. to R-34/in., R-7.8/in. to R-9.2/in., R-6.7/in. to R-7.7/in., and R-4.3/in. to R-4.6/in., respectively, when assuming a 95 % porosity and diminished radiation. To achieve R-10/in., the porosity needed for HFO-filled foam with an anisotropic ratio of 2 is 96.2%, reduced from 97.6% for the isotropic foam design. The improvement in R-value due to anisotropic design is larger at lower porosity and for lower thermal conductivity filler gases. Finally, several strategies to increase the insulation capability of porous polymer foams are provided. These include minimizing radiation contributions, increasing porosity, eliminating CO_2 in the filler gas, and employing anisotropic pores. In essence, this study provides a significant advancement in the field

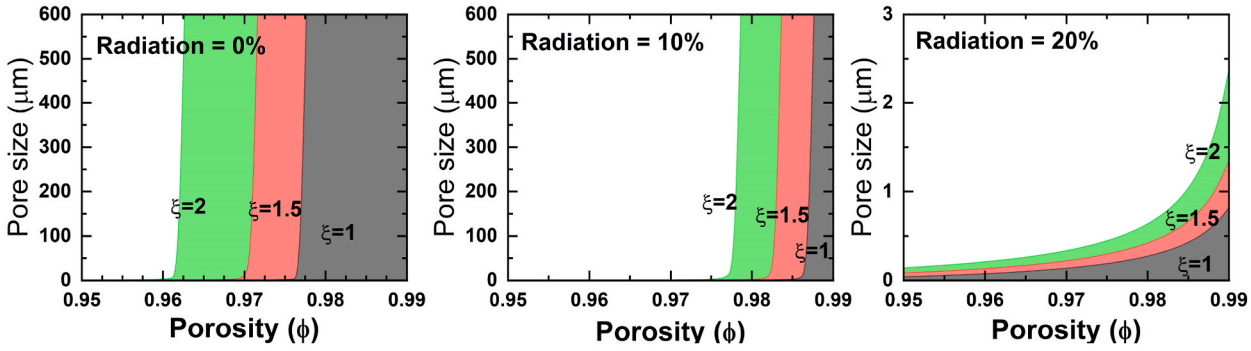

Fig. 9. R-10/in. design space for anisotropic Voronoi polyisocyanurate foam, at (a) 0, (b) 10%, and (c) 20% radiation contribution. The filler gas is HFO.

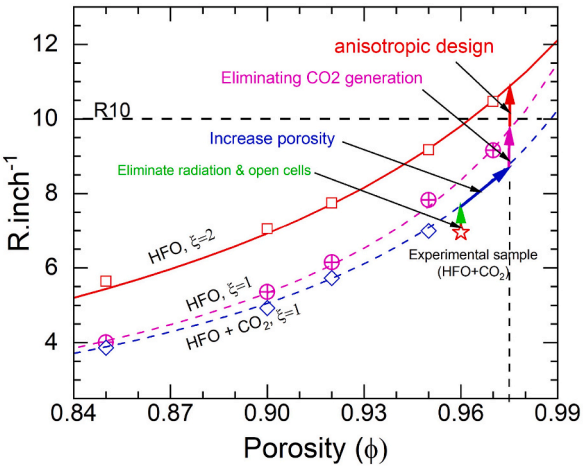

Fig. 10. Various approaches proposed to improve the R-value of the porous polyisocyanurate foam.

of polymer foam design, particularly with anisotropic pore geometry, in achieving ultra-high thermal insulation capability.

Additional information

Correspondence and requests for materials should be addressed to T.F.

CRediT authorship contribution statement

Janak Tiwari: Writing – original draft, Methodology, Investigation, Formal analysis. **Som S. Shrestha:** Writing – review & editing, Supervision, Funding acquisition, Formal analysis, Conceptualization. **Tianli Feng:** Writing – review & editing, Supervision, Resources, Methodology, Investigation, Funding acquisition, Formal analysis, Conceptualization.

Declaration of competing interest

The authors declare the following financial interests/personal relationships which may be considered as potential competing interests:

Som S Shrestha, Tianli Feng reports financial support was provided by US Department of Energy.

Data availability

Data will be made available on request.

Acknowledgments

This research was supported by the US Department of Energy's (DOE's) Office of Energy Efficiency and Renewable Energy (EERE), Building Technologies Office (BTO) under Contract No. DE-AC05-00OR22725 with UT-Battelle, LLC, and used resources at the Building Technologies and Research Integration Center, a DOE-EERE User Facility at Oak Ridge National Laboratory. This work is

supported by the project "Multi-Scale Simulations and Machine Learning-Guided Design and Synthesis of High-Performance Thermal Insulation Materials" funded by the DOE's BTO and EERE.

Appendix A. Supplementary data

Supplementary data to this article can be found online at https://doi.org/10.1016/j.jobe.2024.109717.

References

[1] D. R. Dunn, US Energy Information Administration Monthly Energy Review.
[2] J. Laustsen, P. Ruyssevelt, D. Staniaszek, D. Strong, S. Zinetti, Europe's Buildings under the Microscope, Buildings Performance Institute Europe (BPIE), Brussels, Belgium, 2011.
[3] M.S.M.S. Al-Homoud, Performance characteristics and practical applications of common building thermal insulation materials, Build. Environ. 40 (2005) 353.
[4] B.P.B.P. Jelle, A. Gustavsen, R. Baetens, The path to the high performance thermal building insulation materials and solutions of tomorrow, J. Build. Phys. 34 (2010) 99.
[5] A.M.M. Papadopoulos, E. Giama, Environmental performance evaluation of thermal insulation materials and its impact on the building, Build. Environ. 42 (2007) 2178.
[6] G. M. M. Zaki and A. M. M. Al-Turki, Optimization of Multilayer Thermal Insulation for Pipelines, vol. 21, 63 (n.d.).
[7] C. Jin, Aerogels super-thermal insulation materials by nano hi-tech. Aerogels Handbook 865, 2011.
[8] D.E. Glass, Ceramic matrix composite (CMC) thermal protection systems (TPS) and hot structures for hypersonic vehicles, in: 15th AIAA International Space Planes and Hypersonic Systems and Technologies Conference, 2008.
[9] J.E. Fesmire, Aerogel insulation systems for space launch applications, Cryogenics 46 (2006) 111.
[10] Y. Bao, X. Zhao, The research applications of new heat insulation composite material in automobiles, Heat Tran. Asian Res. 47 (2018) 103.
[11] J.S. Lim, A. Bejan, Two fundamental problems of refrigerator thermal insulation design, Heat Tran. Eng. 15 (1994) 35.
[12] A. Oushabi, S. Sair, Y. Abboud, O. Tanane, A. El Bouari, Natural thermal-insulation materials composed of renewable resources: characterization of local date palm fibers (LDPF), J. Mater. Environ. Sci. 6 (2015) 3395.
[13] U. Kartoglu, J. Milstien, Tools and approaches to ensure quality of vaccines throughout the cold chain, Expert Rev. Vaccines 13 (2014) 843.
[14] G. Dixon, T. Abdel-Salam, P. Kauffmann, Evaluation of the effectiveness of an energy efficiency program for new home construction in Eastern North Carolina, Energy 35 (2010) 1491.
[15] X. Xu, Y. Zhang, K. Lin, H. Di, R. Yang, Modeling and simulation on the thermal performance of shape-stabilized phase change material floor used in passive solar buildings, Energy Build. 37 (2005) 1084.
[16] R. Levinson, H. Akbari, L.M.M. Gartland, E.O.L.O.L. Berkeley, Impact of the temperature dependency of fiberglass insulation R-value on cooling energy use in buildings, Proc. ACEEE 1996 Summer Study on Energy Eff. Buil. 10 (1996) 85.
[17] K.A. Al-Sallal, Comparison between polystyrene and fiberglass roof insulation in warm and cold climates, Renew. Energy 28 (2003) 603.
[18] I.M.M. Ezeonu, J.A.A. Noble, R.B.B. Simmons, D.L.L. Price, S.A.A. Crow, D.G.G. Ahearn, Effect of relative humidity on fungal colonization of fiberglass insulation, Appl. Environ. Microbiol. 60 (1994) 2149.
[19] M. Alam, H. Singh, M.C. Limbachiya, Vacuum insulation panels (Vips) for building construction industry - a review of the contemporary developments and future directions, Appl. Energy 88 (2011) 3592.
[20] S. Brunner, H. Simmler, In situ performance assessment of vacuum insulation panels in a flat roof construction, Vacuum 82 (2008) 700.
[21] H. Simmler, S. Brunner, Vacuum insulation panels for building application: basic properties, aging mechanisms and service life, Energy Build. 37 (2005) 1122.
[22] S. Brunner, K. Ghazi Wakili, T. Stahl, B. Binder, Vacuum insulation panels for building applications - continuous challenges and developments, Energy Build. 85 (2014) 592.
[23] S.E.E. Kalnæs, B.P.P. Jelle, Vacuum insulation panel products: a state-of-the-art review and future research pathways, Appl. Energy 116 (2014) 355.
[24] J. Fricke, U. Heinemann, H.P. Ebert, Vacuum insulation panels-from research to market, Vacuum 82 (2008) 680.
[25] D.M.M. Smith, A. Maskara, U. Boes, Aerogel-based thermal insulation, J. Non-Cryst. Solids 225 (1998) 254.
[26] E. Cuce, P.M.M. Cuce, C.J.J. Wood, S.B.B. Riffat, Toward aerogel based thermal superinsulation in buildings: a comprehensive review, Renew. Sustain. Energy Rev. 34 (2014) 273.
[27] P. Gupta, B. Singh, A.K.K. Agrawal, P.K.K. Maji, Low density and high strength nanofibrillated cellulose aerogel for thermal insulation application, Mater. Des. 158 (2018) 224.
[28] J. Michalak, S. Czernik, M. Marcinek, B. Michalowski, Environmental burdens of external thermal insulation systems. Expanded polystyrene vs. Mineral wool: case study from Poland, Sustainability 12 (2020).
[29] D. Bozsaky, The historical development of thermal insulation materials, Period. Polytechn. Arch. 41 (2010) 49.
[30] T.K. Simon, L. Mlinárik, V. Vargha, Effect of water vapor on the compressive strength of a mineral wool insulation board, J. Build. Phys. 39 (2015) 285.
[31] M. Bogdan, J. Hoerter, F.O. Moore, Meeting the insulation requirements of the building envelope with polyurethane and polyisocyanurate foam, J. Cell. Plast. 41 (2005) 41.
[32] M.C. Basso, X. Li, V. Fierro, A. Pizzi, S. Giovando, A. Celzard, Green, formaldehyde-free, foams for thermal insulation, Adv. Mater. Lett. 2 (2011) 378.
[33] B. Abu-Jdayil, H. Al Abdallah, A. Althabahi, A. Alaydaroos, A. Mlhem, S. Alkhatib, A. El Sayah, H. Hussein, Utilization of polyurethane foam dust in development of thermal insulation composite, Buildings 12 (2022).
[34] D. Feldman, Polymeric foam materials for insulation in buildings. Materials for Energy Efficiency and Thermal Comfort in Buildings 257, 2010.
[35] C.V. Vo, F. Bunge, J. Duffy, L. Hood, Advances in thermal insulation of extruded polystyrene foams, Cell. Polym. 30 (2011) 137.
[36] M. Borowicz, J. Paciorek-Sadowska, J. Lubczak, B. Czupryński, Biodegradable, flame-retardant, and bio-based rigid polyurethane/polyisocyanurate foams for thermal insulation application, Polymers 11 (2019).
[37] P. Buahom, C. Wang, M. Alshrah, G. Wang, P. Gong, M.P. Tran, C.B. Park, Wrong expectation of superinsulation behavior from largely-expanded nanocellular foams, Nanoscale 12 (2020) 13064.
[38] S.S. Shrestha, J. Tiwari, A. Rai, D.E. Hun, D. Howard, A.O. Desjarlais, M. Francoeur, T. Feng, Solid and gas thermal conductivity models improvement and validation in various porous insulation materials, Int. J. Therm. Sci. 187 (2023).
[39] J. Lu, E.A. Lazar, C.H. Rycroft, An Extension to VORO++ for Multithreaded Computation of Voronoi Cells, 2022.
[40] C. Rycroft, Voro++: A Three-Dimensional Voronoi Cell Library in C++, Lawrence Berkeley National Lab.(LBNL), Berkeley, CA (United States), 2009.
[41] V. Gerlich, K. Sulovská, M. Záleśák, COMSOL Multiphysics validation as simulation software for heat transfer calculation in buildings: building simulation software validation, Measurement 46 (2013) 2003.
[42] C. Multiphysics, Introduction to Comsol Multiphysics®, COMSOL Multiphysics, Burlington, MA, 1998. Feb **9**, 32.
[43] J. Tiwari, S. S. Shrestha, T. Feng, T. S. Division, O. Ridge, and O. Ridge, Supplemental Materials for Computational Design of Isotropic and Anisotropic Ultralow Thermal Conductivity Foams, vol. 1 (n.d.).
[44] L. V Nielsen, H.-P. Ebert, F. Hemberger, J. Fricke, A. Biedermann, M. Reichelt, U. Rotermund, *Thermal Conductivity Of Nonporous Polyurethane*, High Temperatures High Pressures(UK), vol. 32, 2000, p. 701.

[45] L.R. Glicksman, Heat transfer and ageing of cellular foam insulation, Cell. Polym. 10 (1991) 276.
[46] M. Santiago-Calvo, J. Tirado-Mediavilla, J.L. Ruiz-Herrero, F. Villafañe, M.Á. Rodríguez-Pérez, Long-term thermal conductivity of cyclopentane–water blown rigid polyurethane foams reinforced with different types of fillers, Polym. Int. 68 (2019) 1826.
[47] N.C. Hilyard, A. Cunningham, Low Density Cellular Plastics: Physical Basis of Behaviour, Springer Science & Business Media, 2012.
[48] J. Kuhn, H.-P. Ebert, M.C. Arduini-Schuster, D. Büttner, J. Fricke, Thermal transport in polystyrene and polyurethane foam insulations, Int. J. Heat Mass Tran. 35 (1992) 1795.
[49] O. Wiener, *Theorie des mischkorpers Fur das feld der stationaren stromung*, abhandl. Sachs. Ges. Wiss, Math. Phys. K1 (1912) 509.
[50] R. Clausius, Die Mechanische Behandlung Der Electricität, vol. 2, Druck und Verlag von Friedrich Vieweg und Sohn, 1879.
[51] J.C. Maxwell, A Treatise on Electricity and Magnetism, vol. 1, Clarendon Press, Oxford, 1873.
[52] H.W.W. Russell, Principles of heat flow in porous insulators, J. Am. Ceram. Soc. 18 (1935) 1.
[53] D.A.G. Bruggeman, The calculation of various physical constants of heterogeneous substances. I. The dielectric constants and conductivities of mixtures composed of isotropic substances, Ann. Phys. 416 (1935) 636.
[54] Z. Hashin, S. Shtrikman, A variational approach to the theory of the effective magnetic permeability of multiphase materials, J. Appl. Phys. 33 (1962) 3125.
[55] T. Mori, K. Tanaka, Average stress in matrix and average elastic energy of materials with misfitting inclusions, Acta Metall. 21 (1973) 571.
[56] K. Raed, Investigation of Knudsen and Gas-atmosphere Effects on Effective Thermal Conductivity of Porous Media, 2013.
[57] F.O. Goodman, Thermal accommodation coefficients, J. Phys. Chem. 84 (1980) 1431.
[58] S.C. Saxena, TRANSPORT PROPERTIES OF GASES AND GASEOUS MIXTURES AT HIGH TEMPERATURES, Univ. of, Illinois, Chicago, 1971.
[59] A. Rai, T. Feng, D. Howard, D. Hun, M. Zhang, H. Zhou, S.S.S.S. Shrestha, Conduction heat transfer through solid in porous materials: a comparative study by finite-element simulations and effective medium approximations, Comput. Therm. Sci. 13 (2021) 19.
[60] R. Hasanzadeh, T. Azdast, A. Doniavi, R.E. Lee, Thermal-insulation performance of low density polyethylene (LDPE) foams: comparison between two radiation thermal conductivity models, Polyolefins J. 6 (2019) 13.
[61] R. Hasanzadeh, T. Azdast, A. Doniavi, Thermal conductivity of low-density polyethylene foams Part II: deep investigation using response surface methodology, J. Therm. Sci. 29 (2020) 159.
[62] F. Hu, S. Wu, Y. Sun, Hollow-structured materials for thermal insulation, Adv. Mater. 31 (2019).
[63] Z. Jia, Z. Wang, D. Hwang, L. Wang, Prediction of the effective thermal conductivity of hollow sphere foams, ACS Appl. Energy Mater. 1 (2018) 1146.
[64] J. You, H. Xing, J. Xue, Z. Jiang, T. Tang, Preparation of rigid cross-linked PVC foam with excellent thermal insulation through adding high-reflectivity IR opacifier, Compos. Sci. Technol. 203 (2021) 108566.
[65] J. You, J. Xue, Z. Jiang, T. Tang, Simultaneously improving thermal insulation, flame retardancy, and smoke suppression for rigid cross-linked polyvinyl chloride foam through combined copper/molybdenum trioxide, Adv. Eng. Mater. 24 (2022) 2100858.
[66] P. Buahom, P. Gong, C. Wang, H. Yu, J. Liu, C.B. Park, Carbon as a solution for nanocellular foam superinsulation, Carbon 189 (2022) 319.
[67] V. Bernardo, E. Laguna-Gutierrez, A. Lopez-Gil, M.A. Rodriguez-Perez, Highly anisotropic crosslinked HDPE foams with a controlled anisotropy ratio: production and characterization of the cellular structure and mechanical properties, Mater. Des. 114 (2017) 83.
[68] V. Bernardo, J. Martin-de Leon, M.A. Rodriguez-Perez, Anisotropy in nanocellular polymers promoted by the addition of needle-like sepiolites, Polym. Int. 68 (2019) 1204.
[69] K.A. Neavor, A.J. Lesser, T.J. McCarthy, *Preparation and Characterization of microcellular polystyrene foams Processed in supercritical CO2*, American chemical society, polymer preprints, Div. Poly. Chem. 38 (1997) 446.
[70] L. Oliveira-Salmazo, A. Lopez-Gil, F. Silva-Bellucci, A.E. Job, M.A. Rodriguez-Perez, Natural rubber foams with anisotropic cellular structures: mechanical properties and modeling, Ind. Crop. Prod. 80 (2016) 26.